1521-009X/42/3/377–383$25.00
Drug Metabolism and Disposition

http://dx.doi.org/10.1124/dmd.113.055988
Drug Metab Dispos 42:377–383, March 2014

Interaction of Human Arylamine *N*-Acetyltransferase 1 with Different Nanomaterials

Zhou J. Deng,[1] Neville J. Butcher, Gysell M. Mortimer, Zhongfan Jia, Michael J. Monteiro, Darren J. Martin, and Rodney F. Minchin

School of Biomedical Sciences (Z.J.D., N.J.B., G.M.M., R.F.M.) and Australian Institute for Biotechnology and Nanotechnology (Z.J., M.J.M., D.J.M.), University of Queensland, Brisbane, Queensland, Australia

Received November 12, 2013; accepted December 17, 2013

ABSTRACT

Humans are exposed to nanoparticles in the environment as well as those in nanomaterials developed for biomedical applications. However, the safety and biologic effects of many nanoparticles remain to be elucidated. Over the past decade, our understanding of the interaction of proteins with various nanomaterials has grown. The protein corona can determine not only how nanoparticles interact with cells but also their biologic effects and toxicity. In this study, we describe the effects that several different classes of nanoparticles exert on the enzymatic activity of the cytosolic protein human arylamine *N*-acetyltransferase 1 (NAT1), a drug-metabolizing enzyme widely distributed in the body that is also responsible for the activation and detoxification of known carcinogens. We investigated three metal oxides (zinc oxide, titanium dioxide, and silicon dioxide), two synthetic clay nanoparticles (layered double hydroxide and layered silicate nanoparticles), and a self-assembling thermo-responsive polymeric nanoparticle that differ in size and surface characteristics. We found that the different nanoparticles induced very different responses, ranging from inhibition to marked enhancement of enzyme activity. The layered silicates did not directly inactivate NAT1, but was found to enhance substrate-dependent inhibition. These differing effects demonstrate the multiplicity of nanoparticle-protein interactions and suggest that enzyme activity may be compromised in organs exposed to nanoparticles, such as the lungs or reticulo-endothelial system.

Introduction

The interaction of proteins and other macromolecules with the surface of nanoparticles has been shown to result in marked changes to the physical properties of the nanoparticles as well as the structure and function of the proteins (Monopoli et al., 2012; Walkey and Chan, 2012). The corona that forms around nanomaterials is comprised of low-affinity, rapidly exchanging proteins and high-affinity, slowly exchanging proteins. The bound proteins can undergo structural rearrangements that alter their function, increase cell surface receptor binding and uptake, or induce undesirable effects such as inflammation, oxidative stress, and cell death. Much of our understanding of the nanoparticle-protein corona has been derived from studies using extracellular media, such as plasma or serum. Less is known about the effect of nanoparticles on intracellular proteins, although many different nanoparticles are taken up into cells (Ryan et al., 2007; Wu et al., 2009; Zhao et al., 2011). Some nanoparticles have already been shown to bind tightly to intracellular proteins such as actin and vimentin (Ehrenberg and McGrath, 2005). Cellular enzymes, particularly those localized to the cytoplasm, will be exposed to nanoparticles that migrate through the cell following uptake. The noncovalent adsorption of enzymes onto various nanoparticles may have profound effects on their behavior (Jordan et al., 2006; Wu et al., 2009; Cruz et al., 2010).

Human arylamine *N*-acetyltransferase 1 (NAT1) is a 33-kDa cytosolic protein with an active site catalytic triad (Sim et al., 2008). Both the crystal structure and the reaction kinetics (Fig. 1, A and B) have been extensively reported (Rodrigues-Lima et al., 2001; Grant, 2008; Butcher and Minchin, 2012), making this enzyme an ideal intracellular candidate to investigate the consequences of nanoparticle-enzyme interactions. NAT1 catalyzes the acetylation of substrates by a one-site ping-pong-bi-bi reaction (Fig. 1B), which requires the cofactor acetyl-coenzyme A (AcCoA). This mechanism commonly exhibits substrate-dependent inhibition at high concentrations because the substrate binds the active site competitively with the cofactor.

Previously, Sanfins et al. showed NAT1 is inactivated when bound to carbon black nanoparticles (Sanfins et al., 2011). Because NAT1 can metabolize many different pollutants, these studies suggested that carbon black may increase susceptibility to chemical toxicity. In this study, we have used a series of unrelated nanoparticles in an attempt to understand the diversity of effects that protein-nanoparticle interactions can elicit using human NAT1 as a model intracellular enzyme.

This work was supported by the National Health and Medical Research Council of Australia [Grants 569694 and APP1024769].

[1]Current affiliation: Koch Institute for Integrative Cancer Research, Massachusetts Institute of Technology, Cambridge, Massachusetts.

dx.doi.org/10.1124/dmd.113.055988.

Materials and Methods

Nanoparticles. Commercial titanium dioxide (TiO_2) nanoparticles (Degussa P25) were purchased from Evonik Degussa (Essen, Germany); silicon dioxide (SiO_2) nanoparticles (S5130) were purchased from Sigma-Aldrich (St. Louis,

ABBREVIATIONS: AcCoA, acetyl-coenzyme A; LDH, layered double hydroxide; LSN, synthetic layered silicate nanoparticles; NAT1, arylamine *N*-acetyltransferase 1; PABA, *p*-aminobenzoic acid; SiO_2, silicon dioxide; TDCN, thermo-responsive diblock copolymer nanoparticles; TiO_2, titanium dioxide; ZnO, zinc oxide.

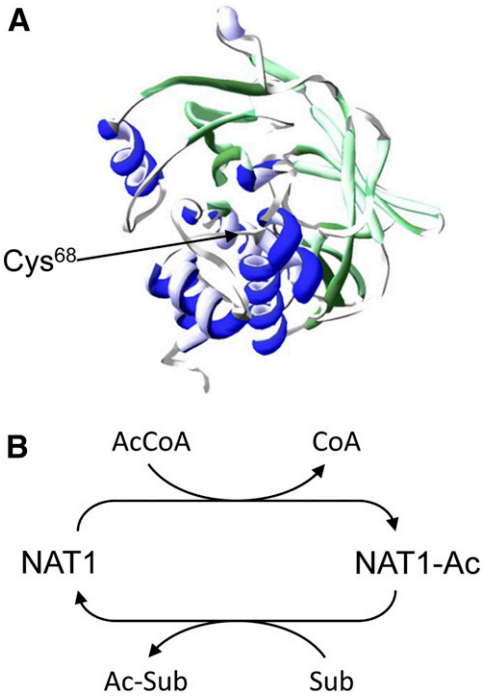

Fig. 1. (A) Ribbon representation of the human arylamine *N*-acetyltransferase crystal structure. The active site catalytic triad resides in a deep cleft. (B) The enzymatic reaction catalyzes the acetylation of substrates by a ping-pong-bi-bi mechanism. The AcCoA initially acetylates the active site cysteine (Cys^{68}), after which the product (CoA) is released. The acetyl group is then transferred to the substrate (Sub), and the resulting product is released. Enzymes that use this reaction mechanism often show substrate-dependent inhibition because, at high concentrations, the substrate competes with the cofactor for binding at the active site.

MO); and zinc oxide (ZnO) nanoparticles (Nanosun 99/30) were supplied by Microniser (Dandenong, VIC, Australia). The characterization of these nanoparticles has been reported elsewhere (Deng et al.). The synthetic layered silicate nanoparticles (LSN) were supplied by Rockwood Additives (Cheshire, UK) (Laponite-RDS) and dispersed into water by 30-minute stirring, followed by 10-minute bath sonication. The synthesis and characterization of layered double hydroxide (LDH) nanoparticles are reported elsewhere (Musumeci et al., 2010). Thermo-responsive diblock copolymer nanoparticles (TDCN) consisting of poly(dimethylacrylamide) and poly(N-isopropylacrylamide) were synthesized, as previously described (Urbani and Monteiro, 2009; Sebakhy et al., 2010). Transmission electron microscopy was performed, as described previously (Deng et al., 2009).

NAT1 Activity. Recombinant human NAT1 protein was expressed and purified, as previously described (Butcher et al., 2004). NAT1 activity was determined using *p*-aminobenzoic acid (PABA) as substrate and AcCoA as cofactor with 10 ng NAT1 protein. *N*-acetylated PABA was quantified by high performance liquid chromatography (Butcher et al., 2000). Reaction rates were determined using variable substrate concentrations and a fixed cofactor concentration (1.1 mM) or variable cofactor concentration and a fixed substrate concentration (0.4 mM). All reactions were performed under linear conditions.

NAT1 Binding. Binding of NAT1 to various nanoparticles was determined in 200 μl buffer (20 mM Tris, 1 mM EDTA, 1 mM dithiothreitol, pH 7.4) at 37°C for 5 minutes, following which the solutions were centrifuged at 200,000*g* at 4°C for 60 minutes. NAT1 alone was used as a control. The unbound proteins in the supernatant were collected and quantified by Western blot and enzyme activity assay.

NAT1 Heat Denaturation. Recombinant NAT1 protein (5 ng/100 μl) was heated to several temperatures between 37°C and 47°C for 10 minutes in the presence and absence of TDCN (5 μg/100 μl). The temperature was then decreased to 37°C, and NAT1 activity was assessed as described above.

Data Analysis and Statistics. All experiments were performed in triplicate. Data are expressed as mean ± S.E.M. Statistical comparisons between different treatments were made using Student's *t* tests. For enzyme kinetics analysis, data were described by the standard Michaelis-Menten equation and parameters (K_m and V_{max}) were estimated by least-squares nonlinear regression analysis (Prism software; GraphPad, San Diego, CA). Kinetic data are presented as Eadie-Scatchard plots.

Results

Inhibition of NAT1 by Nanoparticles. We initially studied the interaction of NAT1 with the metal oxide nanoparticles TiO_2, SiO_2, and ZnO because of their prevalence in products, such as cosmetics and sunscreens, that have confirmed human exposure. These particles have been extensively characterized elsewhere and have been shown to bind a range of serum proteins (Deng et al., 2009). Moreover, metal oxide nanoparticles are rapidly internalized by cells (De Angelis et al., 2013; Jachak et al., 2012), indicating they can interact with intracellular proteins. The Zeta potential for each of the metal oxides (0.5 mg/ml) was similar (−24 to −26 mV) (Deng et al., 2009). However, they varied in size and shape (Fig. 2A). The primary diameter of the TiO_2, SiO_2, and ZnO nanoparticles was 21, 7, and 30 nm, respectively. All three metal oxides agglomerated in buffer to aggregates of 300–450 nm in diameter as determined by dynamic light scattering (Deng et al., 2009). When incubated with NAT1, each of the metal oxide nanoparticles inhibited enzyme activity in a concentration-dependent manner (Fig. 2B), with IC_{50} values of 3–15 μg/ml.

The second class of nanoparticles investigated was the synthetic clays, which included LSN and LDH nanoparticles. These nanomaterials are among the most widely used in industry and are under development as drug delivery systems and in polymer nanocomposites with industrial and biomedical applications (Patel et al., 2006; Pavlidou and Papaspyrides, 2008). Both nanoparticles are comprised of plates approximately 1–2 nm in thickness and 30–100 nm in diameter (Fig. 2A) that assemble to form tactoidal structures. The LSN have a net negative surface charge of −40 mV and a hydrodynamic diameter of 85 nm in solution. By contrast, the LDH have a positive surface charge of +45 mV and a hydrodynamic diameter of 95 nm. When incubated with recombinant NAT1, both synthetic clay nanoparticles inhibited activity (Fig. 2B), but the LSN were significantly more potent (IC_{50} = 0.05 μg/ml versus >1000 μg/ml).

Finally, thermo-responsive diblock copolymer nanoparticles (TDCN) were investigated. These nanoparticles self-assemble at temperatures above their lowest critical solution temperature of ~32°C (Fig. 2A) to form nanoparticles with a diameter of ~30 nm with a narrow particle size distribution (i.e., the polydispersity index was 0.035) and a Zeta potential close to neutral (−0.31 mV) (Urbani and Monteiro, 2009; Sebakhy et al., 2010). When the TDCN were incubated with NAT1, a significant dose-dependent increase in enzyme activity was seen (Fig. 2B). At the highest concentration used (300 μg/ml), activity increased by almost 200% of control.

A plot of the surface Zeta potential against the IC_{50} for each of the metal oxide and clay nanoparticle is shown in Figure 2C. There was a significant positive correlation between these two parameters (R^2 = 0.78, $P < 0.05$), suggesting the inhibition was related to the negative charge of the nanoparticles. We also determined whether the degree of inhibition was directly proportional to the binding of protein to each nanoparticle. For ZnO, LSN, and SiO_2, the percent bound and the percent inhibition of activity were similar (Fig. 2D). However, for the LDH and TiO_2, this was not the case. Both bound ~80% of NAT1 in solution, but activity was only inhibited by 21 and 40%, respectively. These results show that, for the latter nanoparticles, binding does not lead to complete inactivation.

Effect of Metal Oxides on NAT1 Enzyme Kinetics. The effect of each metal oxide on the acetylation of PABA by NAT1 activity was

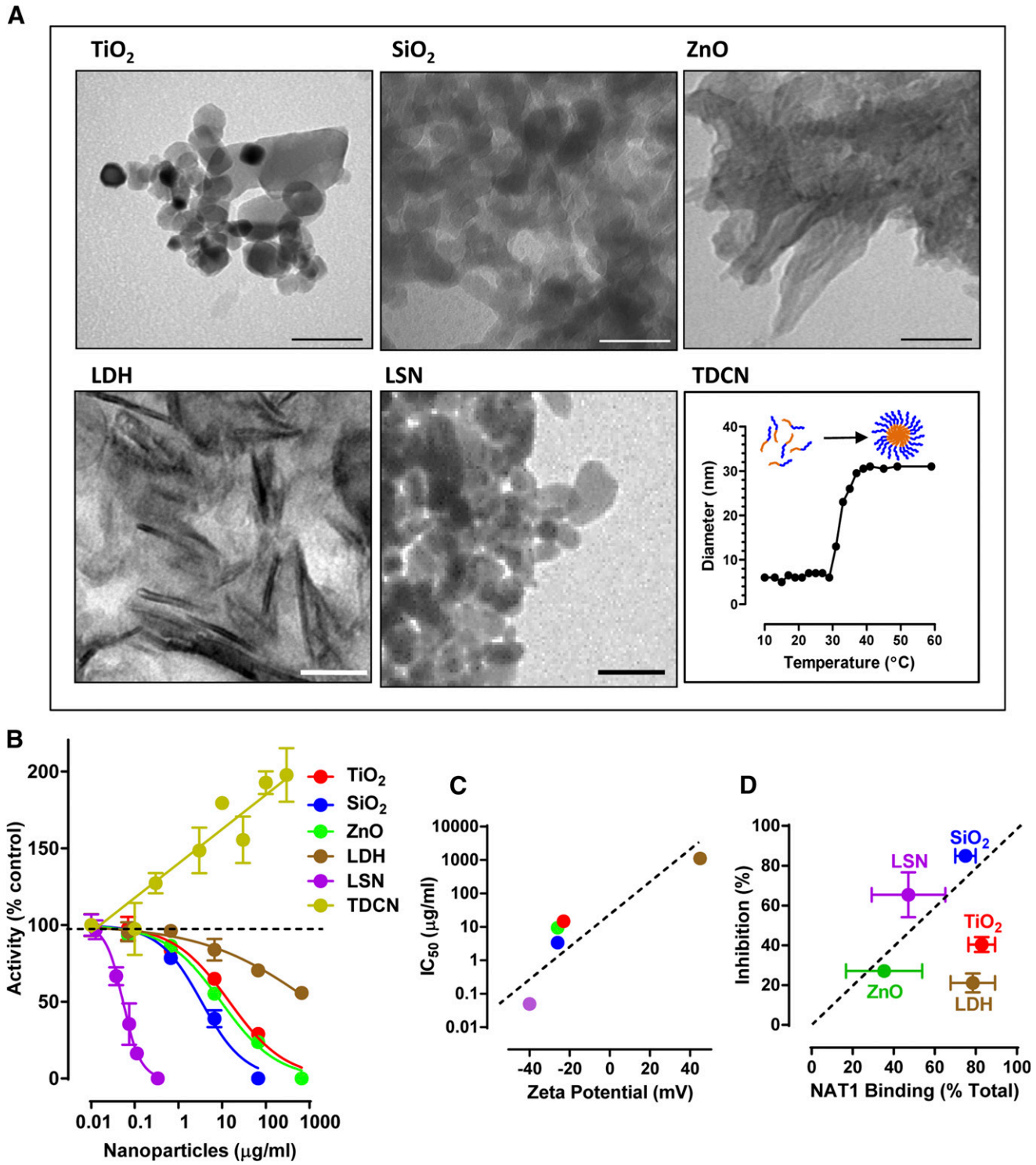

Fig. 2. Inhibition of NAT1 activity by various nanoparticles. (A) Transmission electron micrographs of the different nanoparticles. For the TDCN, the formation of nanoparticles with increasing temperature, as measured by dynamic light scattering, is depicted as these particles could not be imaged by electron microscopy. Bar = 50 nm. (B) Concentration-dependent inhibition of NAT1 activity (0.4 mM PABA and 1.1 mM AcCoA) by the various nanoparticles. Results are mean ± S.E.M., $n = 3$. (C) Correlation between the Zeta potential for each nanoparticle and the IC_{50} determined in (B). Correlation coefficient = 0.78, $P < 0.05$. (D) Plot of the binding of NAT1 to the different nanoparticles versus the percent inhibition of activity. The dotted line represents the line of equivalence. Data are mean ± S.E.M., $n = 3$.

assessed at a fixed nanoparticle concentration. Figure 3 shows Eadie-Scatchard plots for each of the metal oxide nanoparticles where the x intercept represents V_{max} and the slope represents $-1/K_m$, with nontransformed concentration-reaction rate curves shown as inserts. This presentation best illustrates the changes in NAT1 kinetics following binding to the different nanoparticles. The parallel shift to the left in the presence of the three metal oxides (Fig. 3, A–C) is indicative of a decrease in the maximum velocity of the reaction without any significant change in the K_m. This is supported by the estimated kinetic constants determined by nonlinear regression

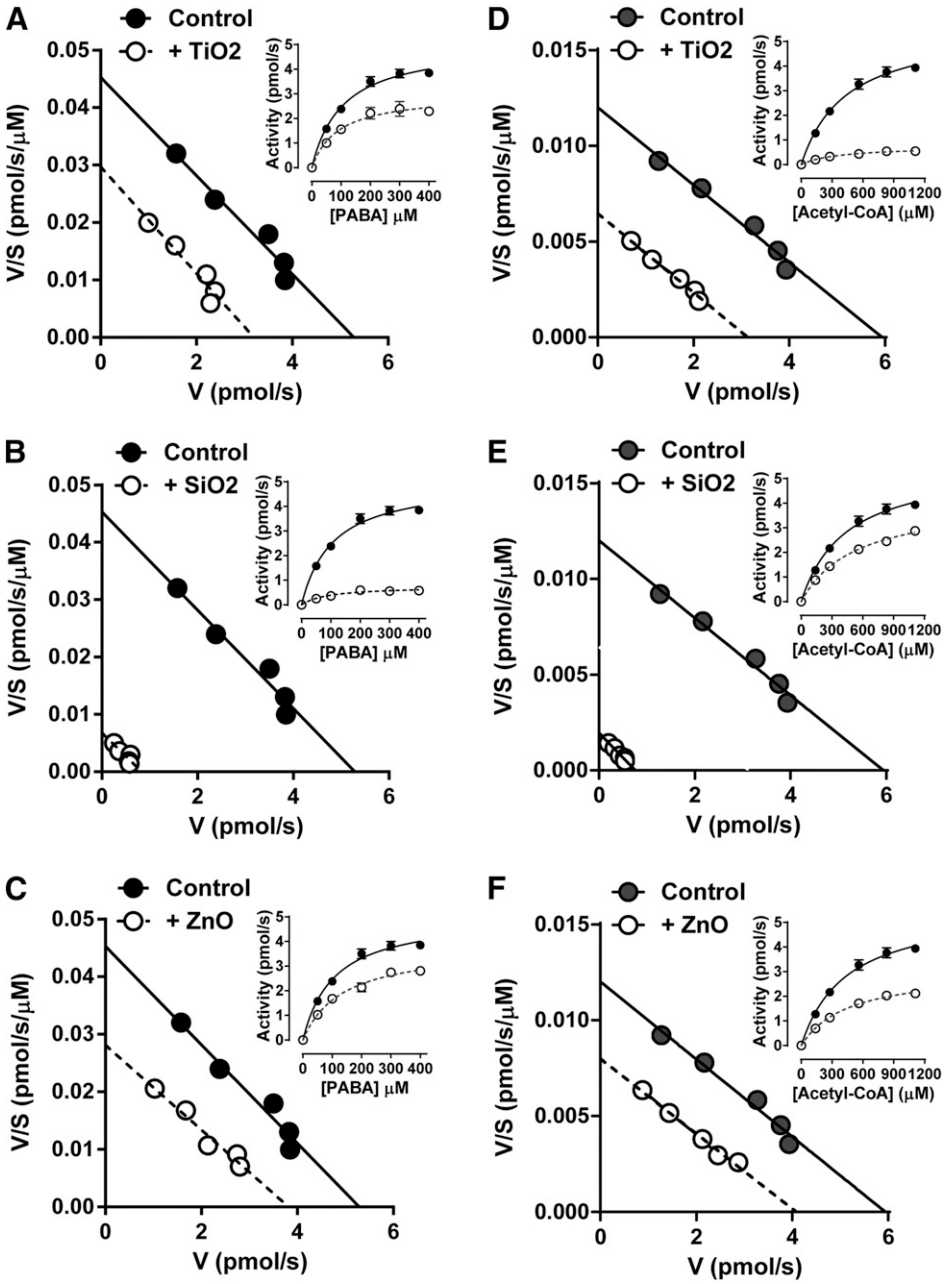

Fig. 3. Eadie-Scatchard plots for NAT1 activity in the presence and absence of the metal oxide nanoparticles. Kinetic curves were determined in the presence of increasing PABA and 1.1 mM AcCoA (A–C) or increasing AcCoA in the presence of 0.4 mM PABA (D–F). Closed circles = no nanoparticle; open circles = plus nanoparticle. Concentration versus activity curves are shown in inserts; data are mean ± S.E.M., $n = 3$.

(Table 1). The kinetics of PABA acetylation was also determined in the presence of increasing cofactor (Fig. 3, D–F). Again, there was a parallel shift to the left in the Eadie-Scatchard plots for the three metal oxides. Taken together, these data are consistent with binding-induced inactivation of the enzyme by these three metal oxides.

Effect of LDH and LSN on NAT1 Enzyme Kinetics. The LDH affected NAT1 activity in a similar manner as the metal oxides with a shift in the Eadie-Scatchard plots to the left (Fig. 4, A and B). By contrast, LSN exhibited a more complex interaction with the enzyme. This was demonstrated by the concave nature of the Eadie-Scatchard plot (Fig. 4C). At low substrate concentration, the rate of acetylation was not altered by the nanoparticle, whereas, at high substrate concentrations, the reaction rate decreased in a dose-dependent manner (Fig. 4C, insert). When the kinetics of the cofactor was examined, similar complex nanoparticle-protein interaction was observed (Fig. 3D). Enzyme activity was not measurable at AcCoA concentrations below 600 μM. The lack of activity at the lower cofactor concentrations was not due to the direct binding of the AcCoA to the nanoparticles because all of it was found in the supernatant following ultracentrifugation of the nanoparticles (data not shown).

The kinetic curves for NAT1 activity in the presence of LSN suggested substrate-dependent inhibition, which has been reported previously for the arylamine *N*-acetyltransferases (Jones et al., 1996). If binding of PABA to the enzyme preceded that for AcCoA, then increasing the concentration of the cofactor should compete for the substrate and result in increased activity. This was seen in Figure 4D (insert). A substrate-dependent inhibition model (Segel, 1975) was fitted to the data by nonlinear least squares regression. For the control (minus nanoparticle), activity was determined up to 800 μM PABA to

TABLE 1

Kinetic parameters for the metabolism of *p*-aminobenzoic acid in the presence of various nanoparticles

Nanoparticle		PABA		AcCoA	
Class	Name	K_m (μM)	V_{max} (pmol/s)	K_m (μM)	V_{max} (pmol/s)
	—	106 ± 16	5.06 ± 0.26	438 ± 63	5.64 ± 0.33
Metal oxides	TiO_2	90 ± 25	2.99 ± 0.27*	456 ± 38	3.08 ± 0.11*
	SiO_2	92 ± 21	0.75 ± 0.06*	370 ± 133	0.74 ± 0.10*
	ZnO	133 ± 22	3.79 ± 0.23*	535 ± 66	4.17 ± 0.23*
Clays	LDH	85 ± 20	3.72 ± 0.27*	486 ± 99	4.49 ± 0.39*
	LSN	N/A	N/A	N/A	N/A
Polymer	TCDN	146 ± 19	10.12 ± 0.53*	298 ± 23*	11.34 ± 0.31*

The Michaelis-Menten equation was fitted to each data set by nonlinear least squares regression (GraphPad). N/A: the data for LSN could not be described by the standard Michaelis-Menten equation (see text).

AcCoA, acetyl-coenzyme A; LDH, layered double hydroxide; LSN, layered silicate nanoparticles; PABA, *p*-aminobenzoic acid; SiO_2, silicon dioxide; TCDN, thermo-responsive diblock copolymer nanoparticles; TiO_2, titanium dioxide; ZnO, zinc oxide.

*Significantly different from control (none), $P < 0.05$.

demonstrate substrate-dependent inhibition. The estimated inhibition constant (K_i) was 1011 ± 262.1 μM in the absence of nanoparticle and 189.7 ± 41.25 μM in its presence. These results show that the interaction of NAT1 with LSN increased the binding of substrate to the enzyme before cofactor bound, suggesting conformational rearrangement of the protein structure.

Effect of TDCN on NAT1 Enzyme Kinetics. The last nanoparticles examined in this study were the self-assembling polymeric nanoparticles TDCN. Unlike any of the other nanoparticles tested, TDCN enhanced the catalytic activity of NAT1 in a dose-dependent manner (Fig. 2B). Kinetic analysis showed a shift to the right in the Eadie-Scatchard plot for PABA metabolism (Fig. 5A) indicative of an increase in the maximum velocity of the reaction with a change in K_m (Table 1). By contrast, there was a shift to the right when the cofactor concentration was varied, but it was not parallel (Fig. 5B). This was because the K_m for AcCoA significantly decreased in the presence of TDCN (Table 1).

NAT1 is sensitive to heat denaturation and showed a significant loss in activity as temperature was increased from 37°C to 47°C (Fig. 5C). However, when incubated with the TDCN, this denaturation was significantly slowed. Taken together, these results suggest the interaction of NAT1 with the TDCN may have induced conformational changes

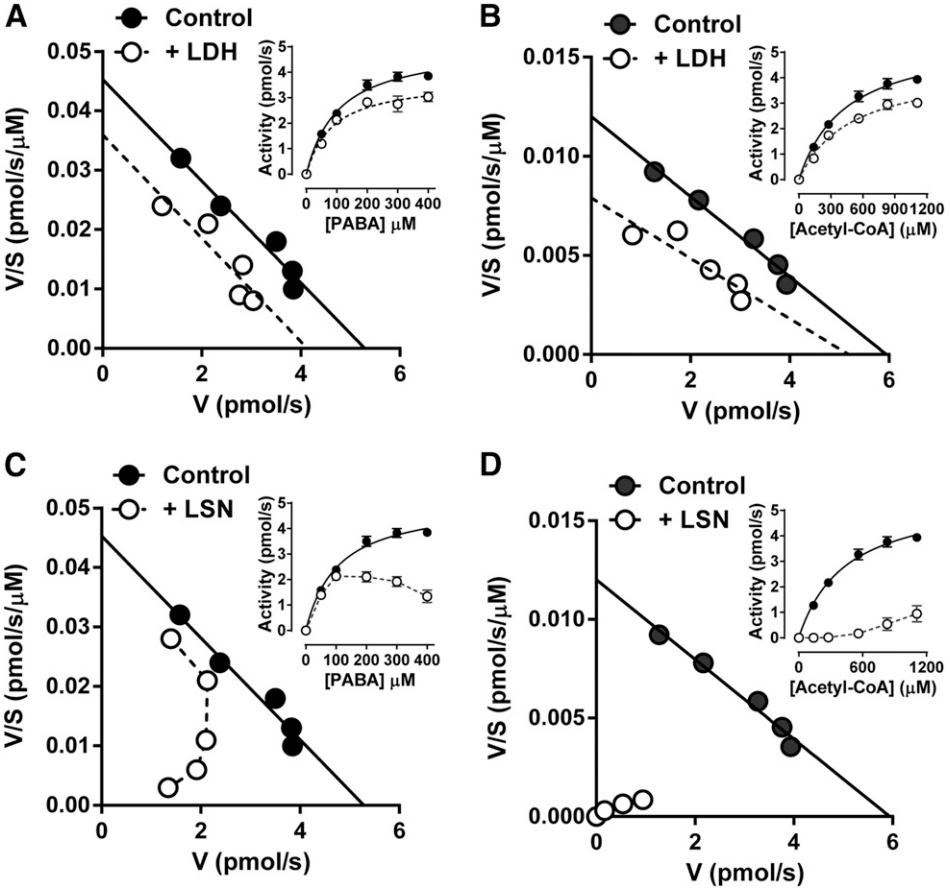

Fig. 4. Eadie-Scatchard plots for NAT1 activity in the presence and absence of LSN and LDH nanoparticles. Kinetic curves were determined in the presence of increasing PABA and 1.1 mM AcCoA (A, C) or increasing AcCoA in the presence of 0.4 mM PABA (B, D). Closed circles = no nanoparticle; open circles = plus nanoparticle. Concentration versus activity curves are shown in inserts; data are mean ± S.E.M., $n = 3$.

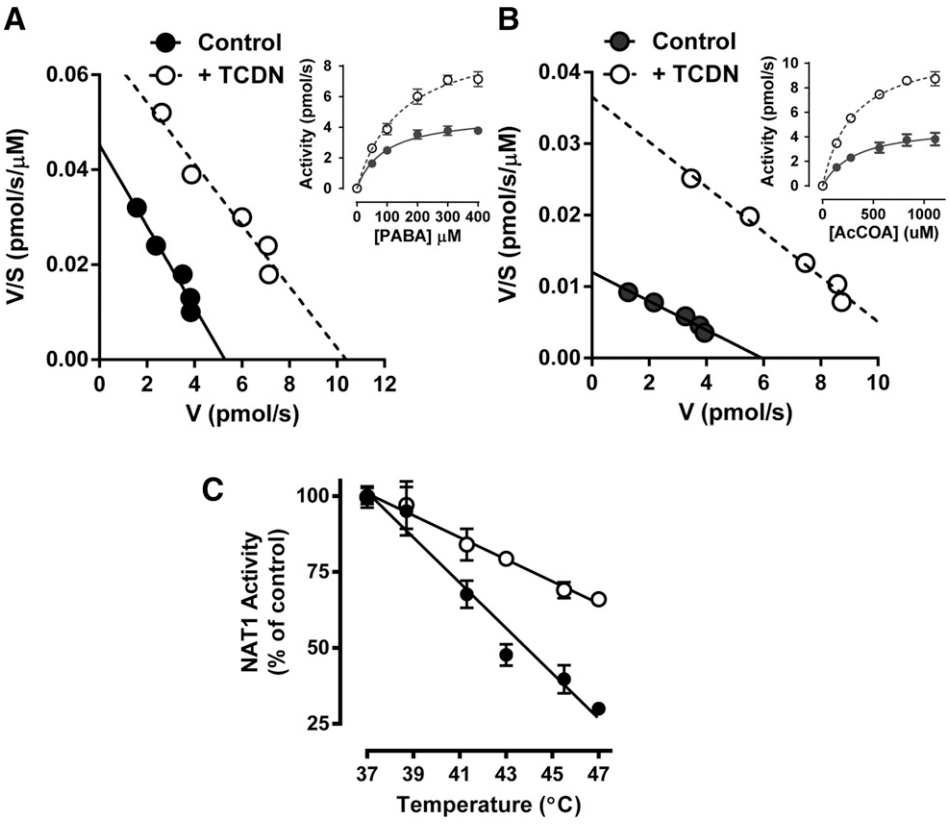

Fig. 5. Effect of TDCN on NAT1 kinetics. (A) Eadie-Scatchard plot for NAT1 activity in the presence of increasing PABA and 1.1 mM AcCoA. (B) Eadie-Scatchard plot for NAT1 activity in the presence of increasing AcCoA and 0.4 mM PABA. Closed circles = no nanoparticle; open circles = plus nanoparticle. Concentration versus activity curves are shown in inserts; data are mean ± S.E.M., $n = 3$. (C) Effect of temperature on NAT1 activity in the absence (closed circles) or presence (open circles) of TDCN. Data are mean ± S.E.M., $n = 3$.

that enhanced the enzymatic efficiency of the protein and appeared to stabilize the enzyme so that it was less susceptible to heat denaturation.

Discussion

In the present study, we examined the effect of various nanoparticles on the reaction kinetics of the cytosolic enzyme NAT1. We showed that different nanoparticles induced different responses ranging from inhibition to enhancement of activity. Moreover, we found that LSN, a class of synthetic clay nanoparticles, altered the enzyme reaction to exacerbate substrate-dependent inhibition. All of these differing effects emphasize the multiplicity of nanoparticle-protein interactions and the range of possible outcomes.

The potency of enzyme inhibition, determined on a weight basis, showed a good correlation with the Zeta potential of the various nanoparticles; more negatively charged nanoparticles associate with lower IC_{50} values. This observation suggests that the nanoparticles inhibit NAT1 activity by binding to positively charged regions of the protein surface. An electrostatic potential map of NAT1 (Swiss-PDB Viewer) reveals a band of positivity around the center of the protein, including the furrow leading to the active site cleft (data not shown). Thus, inhibition of the enzyme by the negatively charged nanoparticles (ZnO, SiO_2, and LSN) may be due to an extensive denaturation of the enzyme on the surface of the nanoparticles, or by the binding interaction occluding the active site. By contrast, although the positively charged LDH bound NAT1 equally or better than the negatively charged particles, they were the least potent in inhibiting activity.

Unexpectedly, we also found that the polymeric TCDN enhanced NAT1 activity and stabilized it against thermal denaturation. TCDN is comprised of poly(dimethylacrylamide) and poly(N-isopropylacrylamide) polymers that self-assemble into nanoparticles above 32°C. These nanoparticles have novel biomedical applications as they can be tuned to take up and release drugs depending on their structure (Chen et al., 2013; Tran et al., 2013). Enhancement of enzyme activity by other nanoparticles has been reported. For example, amino acid-coated gold nanoparticles can activate the cytosolic and membrane-bound forms of carbonic anhydrase (Saada et al., 2011). However, the underlying mechanism remains to be elucidated. This property may have applications in enhancing the activity of target enzymes in various human diseases. Moreover, optimizing enzyme activity and stabilizing the protein may be beneficial in harsh environments such as bioremediation applications and storage of therapeutically active proteins.

Clearly, the results in the present study cannot be inferred to the in vivo environment. Once in the body, the biologic fate of nanoparticles is determined by a complex series of events, such as plasma protein binding, interaction with immune components, distribution through the circulation, interaction with cell membrane, cellular internalization, interactions with intracellular components and proteins, tissue accumulation, and clearance. In the present study, we have attempted to break down this complex process by focusing on one component of the pathway to provide novel insight into nanoparticle-protein interactions. As the number of nanomaterials developed for human use increases, our understanding of their interaction with enzymes and other proteins that affect xenobiotic metabolism will become increasingly important. The current study demonstrates that nanomaterials may have varying effects on enzyme activities. These may be exploited in applications such as bioremediation in which stability and optimum activity are essential, or for the development of enzyme-specific inhibitors, such as fullerene analogs that are potent inhibitors

of the human immunodeficiency virus proteases. Finally, many nanoparticles enter the body via the lungs, a site in which inhibition of enzymes involved in protection from xenobiotics may be particularly critical to overall toxicity.

Authorship Contributions

Participated in research design: Deng, Butcher, Mortimer, Minchin.

Conducted experiments: Deng, Butcher, Mortimer.

Contributed new reagents or analytic tools: Jia, Monteiro, Martin.

Performed data analysis: Deng, Butcher, Minchin.

Wrote or contributed to the writing of the manuscript: Deng, Butcher, Mortimer, Monteiro, Martin, Minchin.

References

Butcher NJ, Arulpragasam A, and Minchin RF (2004) Proteasomal degradation of N-acetyltransferase 1 is prevented by acetylation of the active site cysteine: a mechanism for the slow acetylator phenotype and substrate-dependent down-regulation. *J Biol Chem* **279**: 22131–22137.

Butcher NJ, Ilett KF, and Minchin RF (2000) Substrate-dependent regulation of human arylamine N-acetyltransferase-1 in cultured cells. *Mol Pharmacol* **57**:468–473.

Butcher NJ and Minchin RF (2012) Arylamine N-acetyltransferase 1: a novel drug target in cancer development. *Pharmacol Rev* **64**:147–165.

Chen N, Xiang X, and Heiden PA (2013) Tuning thermoresponsive behavior of diblock copolymers and their gold core hybrids. Part 2. How properties change depending on block attachment to gold nanoparticles. *J Colloid Interface Sci* **396**:39–46.

Cruz JC, Pfromm PH, Tomich JM, and Rezac ME (2010) Conformational changes and catalytic competency of hydrolases adsorbing on fumed silica nanoparticles. I. Tertiary structure. *Colloids Surf B Biointerfaces* **79**:97–104.

De Angelis I, Barone F, Zijno A, Bizzarri L, Russo MT, Pozzi R, Franchini F, Giudetti G, Uboldi C, Ponti J, et al. (2013) Comparative study of ZnO and TiO(2) nanoparticles: physicochemical characterisation and toxicological effects on human colon carcinoma cells. *Nanotoxicology* 7: 1361–1372.

Deng ZJ, Mortimer G, Schiller T, Musumeci A, Martin D, and Minchin RF (2009) Differential plasma protein binding to metal oxide nanoparticles. *Nanotechnology* **20**:455101.

Ehrenberg M and McGrath JL (2005) Binding between particles and proteins in extracts: implications for microrheology and toxicity. *Acta Biomater* **1**:305–315.

Grant DM (2008) Structures of human arylamine N-acetyltransferases. *Curr Drug Metab* **9**: 465–470.

Jachak A, Lai SK, Hida K, Suk JS, Markovic N, Biswal S, Breysse PN, and Hanes J (2012) Transport of metal oxide nanoparticles and single-walled carbon nanotubes in human mucus. *Nanotoxicology* **6**:614–622.

Jones RF, Land SJ, and King CM (1996) Recombinant rat and hamster N-acetyltransferases-1 and -2: relative rates of N-acetylation of arylamines and N,O-acyltransfer with arylhydroxamic acids. *Carcinogenesis* **17**:1729–1733.

Jordan BJ, Hong R, Gider B, Hill J, Emrick T, and Rotello VM (2006) Stabilization of alpha-chymotrypsin at air-water interface through surface binding to gold nanoparticle scaffolds. *Soft Matter* **2**:558–560.

Monopoli MP, Aberg C, Salvati A, and Dawson KA (2012) Biomolecular coronas provide the biological identity of nanosized materials. *Nat Nanotechnol* **7**:779–786.

Musumeci AW, Mortimer GM, Butler MK, Xu ZP, Minchin RF, and Martin DJ (2010) Fluorescent layered double hydroxide nanoparticles for biological studies. *Appl Clay Sci* **48**: 271–279.

Patel HA, Somani RS, Bajaj HC, and Jasra RV (2006) Nanoclays for polymer nanocomposites, paints, inks, greases and cosmetics formulations, drug delivery vehicle and waste water treatment. *Bull Mater Sci* **29**:133–145.

Pavlidou S and Papaspyrides CD (2008) A review on polymer-layered silicate nanocomposites. *Prog Polym Sci* **33**:1119–1198.

Rodrigues-Lima F, Deloménie C, Goodfellow GH, Grant DM, and Dupret JM (2001) Homology modelling and structural analysis of human arylamine N-acetyltransferase NAT1: evidence for the conservation of a cysteine protease catalytic domain and an active-site loop. *Biochem J* **356**: 327–334.

Ryan JA, Overton KW, Speight ME, Oldenburg CN, Loo L, Robarge W, Franzen S, and Feldheim DL (2007) Cellular uptake of gold nanoparticles passivated with BSA-SV40 large T antigen conjugates. *Anal Chem* **79**:9150–9159.

Saada MC, Montero JL, Vullo D, Scozzafava A, Winum JY, and Supuran CT (2011) Carbonic anhydrase activators: gold nanoparticles coated with derivatized histamine, histidine, and carnosine show enhanced activatory effects on several mammalian isoforms. *J Med Chem* **54**: 1170–1177.

Sanfins E, Dairou J, Hussain S, Busi F, Chaffotte AF, Rodrigues-Lima F, and Dupret JM (2011) Carbon black nanoparticles impair acetylation of aromatic amine carcinogens through inactivation of arylamine N-acetyltransferase enzymes. *ACS Nano* **5**:4504–4511.

Sebakhy KO, Kessel S, and Monteiro MJ (2010) Nanoreactors to synthesize well-defined polymer nanoparticles: decoupling particle size from molecular weight. *Macromolecules* **43**: 9598–9600.

Segel IH (1975) *Enzyme Kinetics*, Wiley-Interscience, New York.

Sim E, Walters K, and Boukouvala S (2008) Arylamine N-acetyltransferases: from structure to function. *Drug Metab Rev* **40**:479–510.

Tran NT, Truong NP, Gu W, Jia Z, Cooper MA, and Monteiro MJ (2013) Timed-release polymer nanoparticles. *Biomacromolecules* **14**:495–502.

Urbani CN and Monteiro MJ (2009) Nanoreactors for aqueous RAFT-mediated polymerizations. *Macromolecules* **42**:3884–3886.

Walkey CD and Chan WC (2012) Understanding and controlling the interaction of nanomaterials with proteins in a physiological environment. *Chem Soc Rev* **41**:2780–2799.

Wu Z, Zhang B, and Yan B (2009) Regulation of enzyme activity through interactions with nanoparticles. *Int J Mol Sci* **10**:4198–4209.

Zhao F, Zhao Y, Liu Y, Chang X, Chen C, and Zhao Y (2011) Cellular uptake, intracellular trafficking, and cytotoxicity of nanomaterials. *Small* **7**:1322–1337.

Address correspondence to: Dr. Rodney F. Minchin, School of Biomedical Sciences, University of Queensland, Brisbane, Queensland, Australia. E-mail: r.minchin@uq.edu.au